Numerical analysis of the flame piston-model for acceleration runaway in thin tubes

Raúl Hernández Sánchez, Bruno Denet

Combustion and Flame 270 (2024) 113775

Contents lists available at ScienceDirect

Combustion and Flame

journal homepage: www.sciencedirect.com/journal/combustion-and-flame

Numerical analysis of the flame piston-model for acceleration runaway in thin tubes

Raúl Hernández-Sánchez [a,b,*], Bruno Denet [a]

[a] Aix Marseille Université, CNRS, Centrale Mediterranée, IRPHE UMR7342, Marseille, France
[b] Departamento de Ingeniería Térmica y de Fluidos, Universidad Carlos III de Madrid, 28911 Leganés, Spain

ARTICLE INFO

Keywords:
Deflagration-to-detonation transition
Laminar flame
Thin tubes
Numerical simulation
Finite-time singularity

ABSTRACT

A one-dimensional model is developed and studied to explore the flame acceleration runaway mechanism for deflagration-to-detonation transition in thin tubes. This mechanism relies solely on the thermal feedback between the compression waves ahead of the flame and the temperature-sensitive laminar velocity of the flame. Within this model, the primary driver of the flame acceleration and compressive heating enhancement is the gas flow caused by the increased flame surface area. Results from the numerical integration of the reactive Navier–Stokes equations for perfect gases with a single-step chemical-kinetics model are compared with the solutions obtained when considering the flame as a steady-state discontinuity. The numerical results illustrate the flame acceleration runaway in finite time caused by a double feedback loop established in this model. The evolution of the flame acceleration towards a finite-time singularity eventually leads to the formation of a shock wave within the flame structure, triggering the onset of a detonation.

Novelty and significance statement

This paper presents numerical results obtained using an approach recently proposed to study the effect of flame acceleration on the one-dimensional internal structure of the flame. Unlike previous studies on flame acceleration leading to DDT based on one-dimensional models in which the flame acceleration due to the increase of its surface area is modeled by accelerating chemical kinetics, the present approach consists in the introduction of a backflow of burned gases pushing the flame tip from behind as a piston. The numerical analysis performed in this work allows considering finite reaction rates in this model obtaining results that compare favorably with those obtained when the flame is considered as a discontinuity. The results of this numerical study support previous analytical studies on the flame acceleration runaway mechanism for DDT and illustrate the acceleration process of a flame propagating over a gas flow with a markedly subsonic velocity which leads to the onset of a detonation.

1. Introduction

The Deflagration-to-Detonation (DDT) transition, in which a subsonic flame controlled by diffusion processes abruptly turns into a supersonic reactive wave, represents a critical safety issue in industry [1]. Since its discovery by Mallard and Le Chatelier [2] and Berthelot and Vieille [3], and the pioneering and enlightening experimental campaigns of Urtiew et al. [4], numerous efforts have been devoted to the investigation of this phenomenon and continues to be so, as attested by recent reviews [1,5,6]. Despite the large amount of research, the fundamental mechanism of DDT has not yet been agreed upon. Various forms of DDT have been observed in experiments suggesting different mechanisms (see [7,8] and references therein), but the existence of a universal mechanism remains to discussion.

A first attempt at proposing a universal mechanism was made by Shelkin [9] related to the development of a turbulent flow due to the non-slip condition on the tube walls along which the flame propagates. According to the Shelkin mechanism, turbulence is essential for the flame acceleration which leads to DDT. The theoretical study of the detonation onset in a reactive mixture under the influence of a large reactivity gradient carried out by Zel'dovich et al. [10] was subsequently followed to propose the Shock Wave Amplification through Coherent Energy Release (SWACER) as a mechanism of DDT [11]. A flame acceleration runaway mechanism due to the thermal feedback coupling between the velocity of the flame front and compressible phenomena that could lead to DDT was studied later by Deshaies and Joulin [12]. The Darrieus–Landau (DL) hydrodynamic instability [13,14], which causes an amplification of the perturbations of a planar flame to be

* Corresponding author.
E-mail address: raulhern@ing.uc3m.es (R. Hernández-Sánchez).

https://doi.org/10.1016/j.combustflame.2024.113775
Received 20 September 2023; Received in revised form 24 September 2024; Accepted 26 September 2024
Available online 10 October 2024

further amplified due to the density jump through the flame, has also been proposed as a mechanism of flame acceleration [15,16]. However, recent studies of the DL instability for realistic values of expansion through the flame show that the acceleration induced by this instability in narrow tubes is too short and too weak to initiate a detonation [17, 18]. A different mechanism for DDT based on friction-induced adiabatic compression was proposed by Brailovsky and Sivashinsky [19]. This mechanism, termed hydraulic resistance, has been extensively studied through one-dimensional models [19–21]. The relative impact of flame folding and hydraulic resistance may explain why the detonation onset sometimes occurs inside the tube and sometimes near the tube walls [22]. The present work focuses on the range of tube diameters for which flame folding is the primary mechanism and detonation is formed near the tube axis.

Recent experiments [23–30] and multidimensional direct numerical simulations [24,28,31] have contributed to a more comprehensive understanding of DDT. These studies show consistently a somewhat similar DDT process: (i) a laminar flame propagates subsonically along a tube with a radius on the order of millimeters or a few centimeters, (ii) the flame velocity in a laboratory fixed reference frame increases up to a velocity of the order of the unperturbed sound speed during a flame acceleration phase paired with an increase in flame surface area, (iii) a detonation is originated at a localized point within or close to the internal flame structure. The onset of the detonation is thus a localized phenomenon, and the weak wrinkling of the flame surface at instant of explosion supports the idea that turbulence plays only a supplementary role in flame acceleration, but is not essential [32,33].

The theoretical precursor study of a flame acceleration runaway mechanism for DDT [12] has since been revisited using the square-wave kinetics model [34]. The critical condition for DDT proposed by this analysis, applicable to laminar flames, is based on the non-existence of steady solutions above a critical flame surface area. Deshaies and Joulin [12] derived the steady solutions of a flame-shock ensemble using the weak shock approximation and high thermal sensitivity of the laminar flame speed introducing a flame folding parameter to account for the flame surface wrinkling responsible for flame acceleration. They showed that the thermal feedback of the lead shock wave on the laminar flame velocity introduces criticality conditions that could be the basis for the abrupt transition to a detonation. One-dimensional (1D) numerical simulations [29,34–38] have illustrated this DDT mechanism by means of the Σ model in which the reaction rate is accelerated by a factor Σ^2 to model the flame acceleration due to the increase of flame surface area.

A 1D model of self-accelerating flame [39–41] has been recently proposed and examined. Using this model, the criticality conditions for the flame acceleration runaway mechanism correspond to experimental and numerical observations [39] and are reached under realistic reaction rates. Within this model, described in detail in [39], the flame folding parameter is replaced by a flame elongation parameter. An additional feedback mechanism is introduced through the piston effect of a backflow of burned gas towards the tip of the finger flame which lowers the intensity of the shock wave required to reach criticality.

The self-similar solutions of the flame-shock ensemble have been analyzed in [39]. The self-similar description neglects the dynamics of the compression waves between the flame and the leading shock, assuming the flow in between remains uniform. In the vicinity of the critical point, where the flame acceleration diverges, the uniform flow approximation cannot be accurate due to the rapid flame acceleration. Nonetheless, this model is also suitable for investigating the unsteady compression waves that lead similarly to a finite-time singularity within the experimentally and numerically observed conditions for DDT [40].

This study aims to explore the impact of the backflow of burned gases introduced by the Clavin and Tofaili [39] model on the unsteady internal structure of a 1D flame through numerical integration. This paper first provides a methodology for calculating critical conditions comparable with numerical simulations. Numerical results obtained for the Clavin and Tofaili [39] model using a finite reaction rate are presented hereafter. A 1D unsteady flow of perfect gas has been simulated with the boundary conditions imposed by the piston effect of the backflow of burned gases model through the numerical integration of the macroscopic conservation laws for compressible flows including reactive phenomena. The simulation results illustrate the violent and abrupt flame acceleration along with the shrinking of the internal structure of the flame once the predicted critical flame elongation parameter is surpassed.

2. One-dimensional flame at the tip of an finger flame

2.1. Backflow of burned gases

As in the 1D model of Clavin and Tofaili [39], the expansion of the combustion products produced near the channel walls in the flame skirt is modeled as a mass production term per unit of volume $2\rho_b U_b/R$ along the flame length L, following the approach of Clanet and Searby [42]. Neglecting compressible and unsteady in the region delimited by the closed end, where the gas is at rest, and the flame tip, the conservation of mass leads to a backflow of burned gas that impinges the flame tip from behind with velocity

$$u_b = SU_b. \tag{1}$$

Here, the elongation parameter S is proportional to the ratio of the flame length L to the tube radius R. For instance, for a simplified description of a flame envelope given by the surface of a cylinder, as that of [42], the elongation parameter would be expressed as $S = 2L/R$. However, the exact relationship between the flame length and the elongation parameter defining the gas flow is out of the scope of this work. The subsequent analysis is limited to assess the evolution of flame acceleration when the elongation parameter defined in Eq. (1) is increased. The backflow of gases drives the flame acceleration in the 1D model (see Fig. 1) for finger flames, $R/L \ll 1$. A qualitatively similar flow field is observed through Particle Image Velocimetry (PIV) in an insightful experimental analysis [43] as well as in two-dimensional numerical simulations [44].

Both the σ and S parameters from the analysis of Deshaies and Joulin [12] and Clavin and Tofaili [39] model, respectively, provide a quantitative measure of the ratio of flame surface to normal section in the direction of propagation which controls the flame propagation velocity $u_f = \sigma U_b = (S+1)U_b$. The latter formulation of Clavin and Tofaili [39] might be interpreted as a reformulation of the Deshaies and Joulin [12] model. While multidimensional effects are averaged over the tube cross section in the σ model, the S model is limited to elongated flames and analyzes the flame tip internal structure. The multidimensional character of the flame is introduced in the S model by the backflow of burned gases originating from the flame skirt pushing forward the flame tip. Therefore, numerical studies based on the analysis of Deshaies and Joulin [12] for one-dimensional models performed so far, such as [34,36], consider the multidimensional effects of an increased flame surface area by increasing the reaction rate. Based on the Clavin and Tofaili [39] model, a different approach is proposed in this work to study the internal structure of the flame tip during the subsonic flame acceleration runaway predicted originally by Deshaies and Joulin [12].

2.2. Governing equations

The dynamics of unsteady propagation of a 1D deflagration are described by the Navier–Stokes equations supplemented with the conservation laws of mass, energy and chemical species. The governing equations for the conservation of mass

$$\frac{\partial \rho}{\partial t} + \frac{\partial (\rho u)}{\partial r} = 0, \tag{2}$$

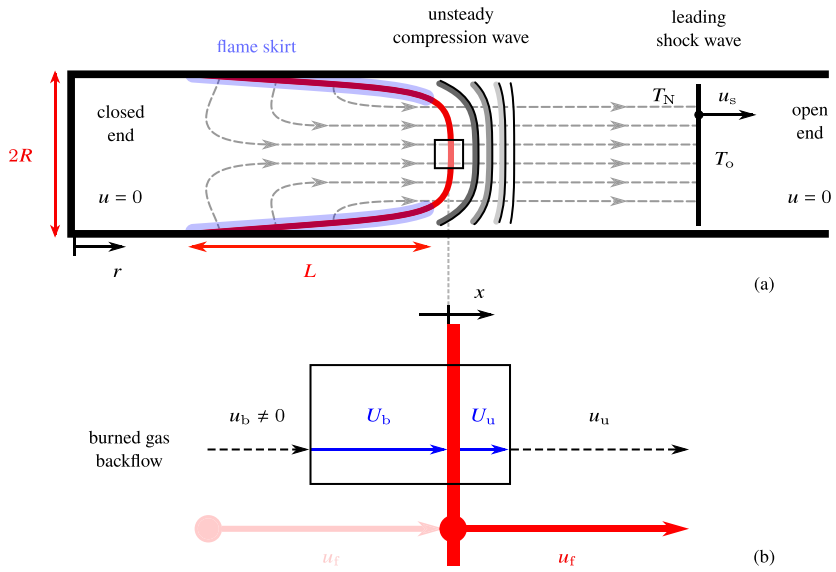

Fig. 1. (a) Sketch of the finger flame model of Clavin and Tofaili [39]. The streamlines are represented by light black dashed lines with arrows, while the flame surface is depicted by the thick red line, with the flame skirt highlighted in light blue. (b) One-dimensional model at the tip of the flame with the absolute flow velocities represented by dashed black arrows and the flame velocities with respect to the flow by blue arrows.

momentum

$$\frac{\partial(\rho u)}{\partial t}+\frac{\partial\left(\rho u^2\right)}{\partial r}+\frac{1}{\gamma M_{\mathrm{bo}}^2}\frac{\partial p}{\partial r}=\mathrm{Pr}\,\frac{\partial^2 u}{\partial r^2}, \tag{3}$$

total energy

$$\frac{\partial(\rho E)}{\partial t}+\frac{\partial(\rho u E)}{\partial r}+\frac{\gamma-1}{\gamma}\frac{\partial(p u)}{\partial r}$$
$$=\frac{\partial^2 T}{\partial r^2}+M_{\mathrm{bo}}^2\,\mathrm{Pr}(\gamma-1)\frac{\partial}{\partial r}\left(u\frac{\partial u}{\partial r}\right)+\rho q\omega \tag{4}$$

and reactant mass fraction

$$\frac{\partial(\rho Y)}{\partial t}+\frac{\partial(\rho Y u)}{\partial r}=\frac{1}{\mathrm{Le}}\frac{\partial^2 Y}{\partial r^2}-\rho\omega \tag{5}$$

are written here the dimensionless spatial coordinate system of the tube $r = r'/l'_{\mathrm{fo}}$ and dimensionless time coordinates $t = t'/t'_{\mathrm{fo}}$ where $l'_{\mathrm{fo}} = D'_{\mathrm{Tbo}}/U'_{\mathrm{bo}}$ is the characteristic length scale of the flame thickness, D'_{Tbo} denotes the thermal diffusivity of the burned gases, U'_{bo} is velocity of a flame with respect to the burned gases propagating in a mixture initially at unperturbed temperature T'_{o} and $t'_{\mathrm{fo}} = l'_{\mathrm{fo}}/U'_{\mathrm{bo}}$ represents the corresponding transit time. The physical quantities of density $\rho = \rho'/\rho'_{\mathrm{bo}}$, flow velocity $u = u'/U'_{\mathrm{bo}}$, pressure $p = p'/p'_{\mathrm{o}}$, temperature $T = T'/T'_{\mathrm{bo}}$, total energy $E = E'/(c'_{\mathrm{p}}T'_{\mathrm{bo}})$ and heat of reaction $q = q'_{\mathrm{m}}Y'_{\mathrm{o}}/(c'_{\mathrm{p}}T'_{\mathrm{bo}})$ are made dimensionless with the state of the burned gas behind a flame propagating from the open end of a tube, i.e. $T'_{\mathrm{bo}} = T'_{\mathrm{o}} + q'_{\mathrm{m}}Y'_{\mathrm{o}}/c'_{\mathrm{p}}$, and the reactant mass fraction is normalized with its initial value $Y = Y'/Y'_{\mathrm{o}}$. The nondimensional Prandtl $\mathrm{Pr} = \mu'/(\rho'_{\mathrm{b}}D'_{\mathrm{Tb}})$ and Lewis $\mathrm{Le} = D'_{\mathrm{T}}/D'$ numbers appear naturally in the dimensionless equations to quantify the relative contribution of the different molecular diffusion effects. The thermophysical properties of specific heat capacity at constant pressure c'_{p} and constant volume c'_{v} and thermal conductivity are considered to remain constant, leading to the relation $\rho' D'_{\mathrm{T}} = \rho'_{\mathrm{bo}}D'_{\mathrm{Tbo}}$ that defines the thermal diffusivity. An equation of state for perfect gases is applied $p' = \left(c'_{\mathrm{p}} - c'_{\mathrm{v}}\right)\rho' T'$, which in the chosen units is written as $p = \rho T$ while the speed of sound is $a^2 = T/M_{\mathrm{bo}}^2$, where $M_{\mathrm{bo}} \equiv U_{\mathrm{bo}}/a_{\mathrm{bo}}$ is the flame Mach number relative to the burned gases. The total energy, which accounts for the internal thermal energy $e' = c'_{\mathrm{v}}T'$ and the macroscopic kinetic energy $u'^2/2$, is written as $E = T/\gamma + M_{\mathrm{bo}}^2(\gamma-1)u^2/2$, where $\gamma = c'_{\mathrm{p}}/c'_{v} = 1.4$ represents the heat capacity ratio. A single-step reaction model $\mathrm{R}\xrightarrow{\omega}\mathrm{P}$ is employed whose chemical-kinetics reaction rate obeys an Arrhenius law

$$\omega = \frac{\omega'}{1/t'_{\mathrm{fo}}} = \frac{\beta_{\mathrm{o}}^{\vartheta+1}}{2\vartheta!\mathrm{Le}^{\vartheta}}\rho^{\vartheta}Y^{\vartheta}\exp\left[\frac{E_{\mathrm{a}}}{\mathrm{k_B}T_{\mathrm{bo}}}\left(1-\frac{1}{T}\right)\right], \tag{6}$$

where ϑ and E_{a} are the order and the activation energy of the reaction model, and $\mathrm{k_B}$ is the Boltzmann constant relating the thermal energy of a gas with the thermodynamic temperature. For clarity, the Zeldovich number, β_{o}, that provides a quantitative measure of the reaction rate sensitivity to temperature and is defined as the product of dimensionless activation energy and heat of reaction

$$\beta_{\mathrm{o}} \equiv \frac{E_{\mathrm{a}}}{\mathrm{k_B}T_{\mathrm{bo}}}\frac{q_{\mathrm{m}}}{c_{\mathrm{p}}T_{\mathrm{bo}}}, \tag{7}$$

has been introduced.

3. Double-discontinuity model

The propagation of a flame through a reactive mixture induces a movement of the surrounding gas. This motion is caused by the difference in flow velocity on both sides of the flame, which is generated to satisfy mass conservation taking into account the lower density of the burned gases with respect to the fresh mixture. When a flame is initiated at the closed end of a tube, the induced flow by the expansion of the burned gases leads to the formation of a shock wave ahead of the flame. The distance between the flame and the shock wave grows linearly with time at a rate given by the difference between the absolute flame propagating velocity $u_{\mathrm{f}} \equiv \mathrm{d}r_{\mathrm{f}}/\mathrm{d}t$ and that of the shock wave $u_{\mathrm{s}} \equiv \mathrm{d}r_{\mathrm{s}}/\mathrm{d}t$. Under ordinary conditions, a flame propagates with a markedly subsonic velocity $u_{\mathrm{f}}/a_{\mathrm{o}} \ll 1$ while a shock wave propagates faster than the sound speed $u_{\mathrm{s}}/a_{\mathrm{o}} > 1$ resulting in large velocity difference $u_{\mathrm{f}}/u_{\mathrm{s}} \ll 1$. Therefore, at the length scale given by the size of the shock-flame complex both the shock wave and the flame can be considered as discontinuities soon after ignition.

Across the shock wave, the gas temperature increases from the initial temperature T_{o} to the temperature at the Neumann state T_{N}. Likewise, the gas flow, considered still ahead of the shock wave, moves with a velocity u_{N} behind the shock wave in the propagation direction of the supersonic discontinuity. The values of the temperature ratio and the flow velocity can be obtained through integration of the conservation equations of mass, momentum and total energy Eqs. (2)–(4) in the

moving reference frame of the shock wave. These relationships are the well-known Rankine–Hugoniot jump conditions

$$\frac{T_N}{T_o} = \frac{\left[2\gamma M_o^2 - (\gamma-1)\right]\left[(\gamma-1)M_o^2+2\right]}{(\gamma+1)^2 M_o^2} \tag{8}$$

$$\frac{u_N}{a_o} = \frac{2}{\gamma+1}\left(M_o - \frac{1}{M_o}\right) \tag{9}$$

which provide the temperature jump and flow velocity to sound speed ratio in terms of the shock wave Mach number $M_o \equiv u_s/a_o$.

Within the internal structure of a steady flame, mass conservation Eq. (2) requires mass flux to remain constant

$$\rho_u U_u = \rho_b U_b, \tag{10}$$

and the absolute flame propagating velocity u_f can be decomposed into the flow velocity u and the velocity of the flame relative to the flow U

$$u_f = u_u + U_u = u_b + U_b, \tag{11}$$

where the subscripts u and b denotate respectively the flow ahead and behind the flame.

The thermal propagation of the flame which governs the flame velocity relative to the flow results in a markedly subsonic flame $M_b = U_b/a_b \ll 1$. Thus, since pressure variations in the quasi-steady regime are proportional to the square of the Mach number $\Delta p \sim M_b^2$ (see Eq. (3)), the flame can be considered to be isobaric

$$p = \rho_u T_u = \rho_b T_b. \tag{12}$$

Integration of the energy conservation Eq. (4) along the isobaric flame structure leads to the classical expression for the adiabatic flame temperature

$$T_b = T_u + q. \tag{13}$$

According to the asymptotic analysis of thermal flame propagation in the limit of large activation energy $\beta_o \to \infty$ by Zeldovich and Frank-Kamenetskii [45], the laminar flame velocity relative to the flow of gases is strongly sensitive to temperature. As discussed in [7,39], the dependence of the laminar flame velocity U_L on the burned gas temperature T_b for the reaction rate described by Eq. (6) in the large activation energy asymptotic limit yields

$$U_b = U_L(T_b) = T_b^{\vartheta+1} \exp\left[\frac{E_a}{2k_B T_{bo}}\left(1 - \frac{1}{T_b}\right)\right] \tag{14}$$

3.1. Self-similar solutions

Considering the initial phase of flame acceleration when flame velocity grows on a time scale much larger than the acoustic time, the flow between the flame and the shock wave can be accurately assumed to be uniform. Acoustic waves propagating back and forth between the flame and the shock uniformize the state variables of the flow. In this scenario, the temperature and the flow velocity of the unburned gas ahead of the flame are given by the Neumann state just behind the shock wave,

$$T_u = T_N \quad \text{and} \quad u_u = u_N. \tag{15}$$

Moreover, since both waves are considered as discontinuities, the only length scale left in the problem is the distance between the waves. When both waves propagate with constant velocity, the distance that separates them is a linear function of time. Therefore, the problem actually lacks spatial scales and a solution dependent on the dimensionless self-similar variable x/t can be found.

The system of Eqs. (8)–(15) provides the nonlinear relationship between the flame velocity u_f and the elongation parameter S that characterizes the self-similar solution for given set of thermochemical properties of the reactive mixture including the reaction heat q, the dimensionless activation energy β, the reaction order ϑ and the burning flame Mach number relative to the burned gases M_{bo}. This relationship can be obtained numerically, without more approximations, using the shock wave Mach number M_o as a parameter and pairing up the corresponding flame velocity u_f and elongation parameter S.

Examples of the relationships between flame velocity and the elongation parameter for different parametric values of the thermochemical properties are depicted in Fig. 2. Characteristic values for reactive mixtures that exhibit DDT when a flame propagates along a tube free of obstacles, such as hydrogen-oxygen and ethylene-oxygen (see [25]), have been considered here. A reference set of parameters $\vartheta = 2$, $q = 0.875$, $M_{bo} = 2\times10^{-2}$ and $\beta_o = 10$ is considered unless otherwise indicated and every parameter is increased or reduced within its range of typical values. Although quantitative differences are observed depending on the model parameters, all curves show a qualitatively similar behavior. The existence of a critical elongation value above which no steady solution exists is common to all of them. As in the theoretical analysis of Deshaies and Joulin [12], two solution branches that collapse on the turning point can be identified. Regardless of the value of the thermochemical parameters, the ratio between the critical flame velocity at the turning point and the unperturbed sound speed remains on the order of order unity. As noted in [39], where an alternative approach based on the tangency of two curves obtained using the approximation $2\gamma M_o^2/(\gamma-1) \ll 1$ was followed, the critical flame velocities yielded by this model are of the order of the initial sound speed, as has been reported in experimental studies (see Fig. 8 in [25]). The critical elongation, given by the elongation at the turning point, follows an inverse relation with the reaction order (Fig. 2(a)), the burning velocity of the flame (Fig. 2(c)), and the activation energy (Fig. 2(d)), while it decreases with the reaction heat (Fig. 2(b)). In Fig. 2(c), it can be observed the strong dependence of the critical flame elongation parameter on the burning velocity of the flame, which might explain why this runaway flame acceleration mechanism is not observed in less reactive mixtures characterized by slower burning velocities.

3.2. Accelerating flame in an isentropic flow

The self-similar solutions, which assume a uniform flow between the flame and the leading shock wave, cannot accurately describe the flow evolution in the vicinity of the turning point, where a fast flame acceleration is predicted as it approaches the finite-time singularity [40]. As the characteristic time of flame acceleration approaches the acoustic time, the flow between the shock wave and the flame can no longer be considered uniform, i.e. $u_u \neq u_N$ and $T_u \neq T_N$. The compression waves emitted from the flame modify the conditions ahead of the flame with respect to the conditions behind the shock wave.

By limiting the scope of the study to situations for which the unsteady compression waves do not reach the shock wave and do not generate an intermediate shock wave, the flow between the shock wave and the flame can be considered isentropic. Therefore, the relationship between the temperature ahead of the flame T_u and behind the shock T_N is determined by the upstream Riemann invariant $J_- = u_N - 2/(\gamma-1)\,a_N = u_u - 2/(\gamma-1)\,a_u$ and it is expressed as

$$\frac{T_u}{T_N} = \left[1 + \frac{\gamma-1}{2}\frac{u_N}{a_N}\left(\frac{u_u}{u_N} - 1\right)\right]^2. \tag{16}$$

The nonlinear relationship between the flame velocity and the elongation parameter for a given set of thermochemical properties of the reactive mixture γ, q, β, ϑ and M_{bo}, and a far shock wave with a given intensity M_o when an isentropic compression wave is allowed to develop within the shock-flame complex is determined by the system of Eqs. (8)–(14) and (16). This relationship can be determined numerically without added approximations utilizing the ratio of the flow velocity ahead of the flame to the flow velocity behind the shock wave u_u/u_N as a parameter and matching the elongation parameter that corresponds to each absolute flame velocity.

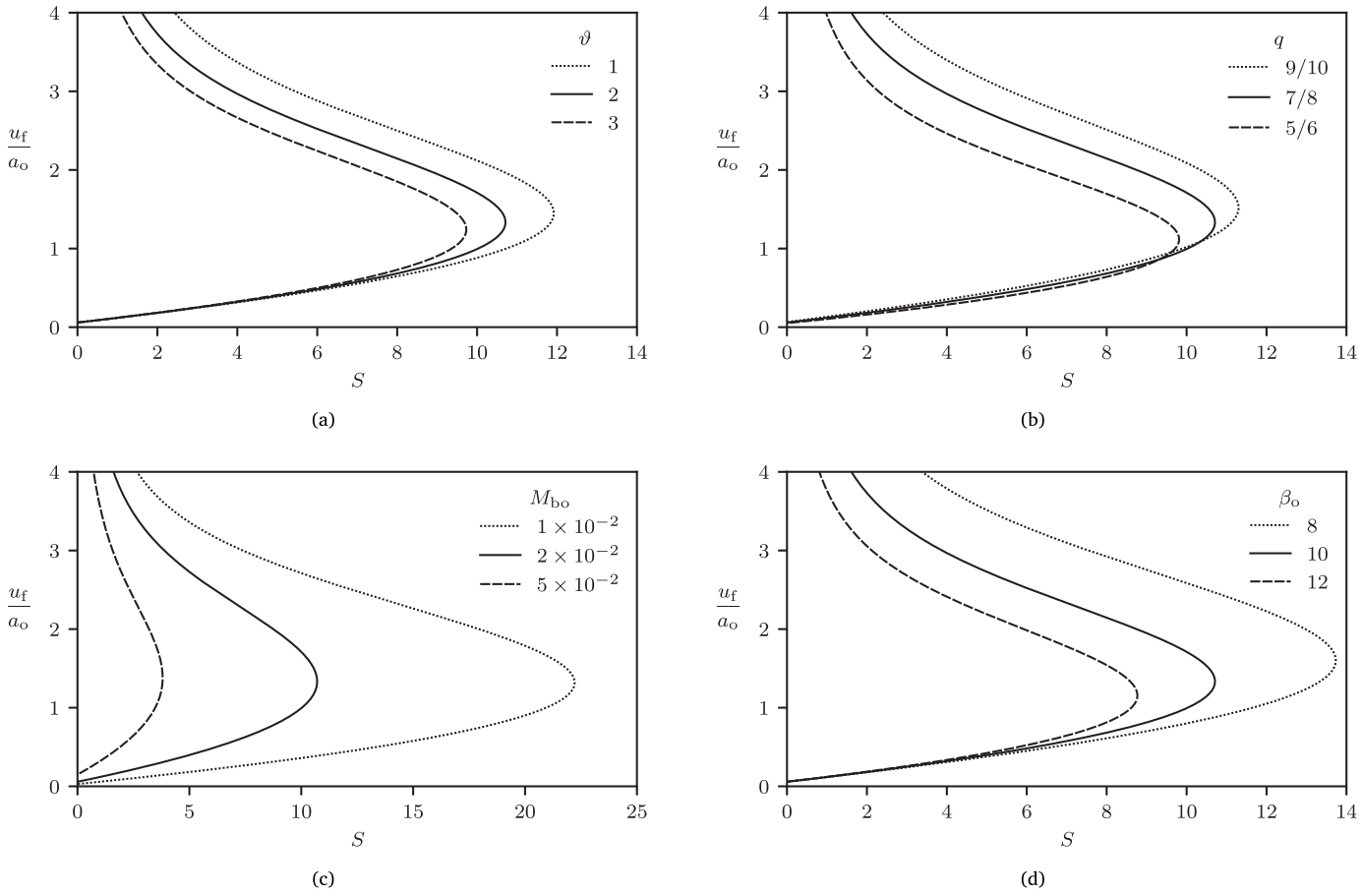

Fig. 2. Nonlinear relationships between the absolute flame propagating velocity to sound speed ratio u_f/a_o and the flame elongation parameter S in the self-similar solutions of the double discontinuity model. Thermochemical parameters take numerical values of $\vartheta = 2$, $q = 7/8 = 0.875$, $M_{bo} = 2 \times 10^{-2}$ and $\beta_o = 10$ unless otherwise indicated in the figure legend.

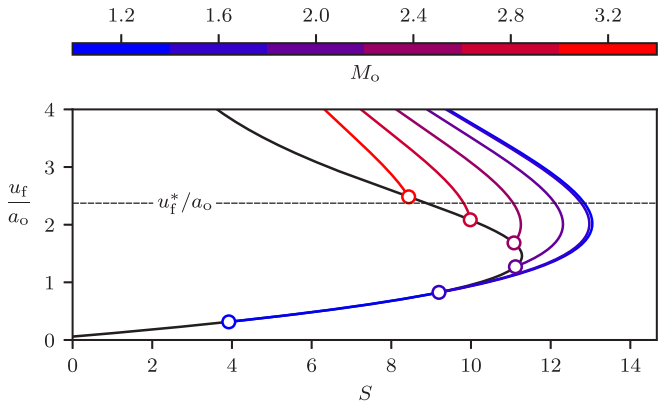

Fig. 3. Nonlinear relationships between the absolute flame propagating velocity to sound speed ratio u_f/a_o and the flame elongation parameter S when the development of isentropic compression waves is considered within the double discontinuity model for the set thermochemical properties $q = 0.875$, $\beta_o = 10$, $\vartheta = 2$ and $M_{bo} = 2 \times 10^{-2}$ and different values of the shock wave Mach number $M_o = 1.2, 1.6, 2.0, 2.4, 2.8$ and 3.2 (blue to red lines). The empty circles highlight the relationship when the flow is uniform, $u_u = u_N$, for the given shock wave Mach number, i.e. the solution that lies on the self-similar curve (black line). (For interpretation of the references to color in this figure legend, the reader is referred to the web version of this article.)

The curves representing the relationship between the absolute flame velocity and the elongation parameter are presented in Fig. 3 for a specific reactive mixture with $q = 0.875$, $\beta_o = 10$, $\vartheta = 2$ and $M_{bo} = 2 \times 10^{-2}$ considering different values of the far shock wave intensity M_o. As for the self-similar solutions, it is observed that there is a maximum value of flame elongation above which there is no solution. It can be noted that the critical absolute flame velocity is independent of the leading shock intensity. Consequently, when the flame velocity of the corresponding self-similar solution is below the new critical flame velocity a turning point appears separating the two branches of flame velocity solutions for a given flame elongation. Conversely, for faster flame velocities, only the upper branch persists, and the curve exhibits no turning point. It is also noteworthy that in cases where the self-similar solution is located in the lower branch, the critical flame elongation is consistently larger than the critical elongation of the self-similar solutions. Nevertheless, the more intense the far shock wave, the smaller the critical flame elongation. These results are in good qualitative agreement with the analytical description under the approximation $u_f/a_o \ll 1$ [40].

Neglecting the prefactor in front of the exponential term in Eq. (14) for a large activation energy, as well as considering small variations of the burned gas temperature $T_b - 1 \ll 1$, large elongation $S \gg 1$ and weak far shock wave $M_o - 1 \ll 1$, the nonlinear relationship between flame velocity and elongation given by Eqs. (8)–(14) and (16) simplifies to

$$u_f \approx S \exp\left[\tilde{b}\frac{\gamma-1}{a_o}u_f + \tilde{b}\left(\frac{\gamma-1}{2a_o}u_f\right)^2\right], \tag{17}$$

where the thermal sensitivity parameter $\tilde{b} \equiv T_u/U_b\, dU_b/dT_u = E_a/(2k_B T_{bo})\, T_o/T_{bo}$ proposed in [40] has been introduced. Under the aforementioned approximations, an expression for the critical flame

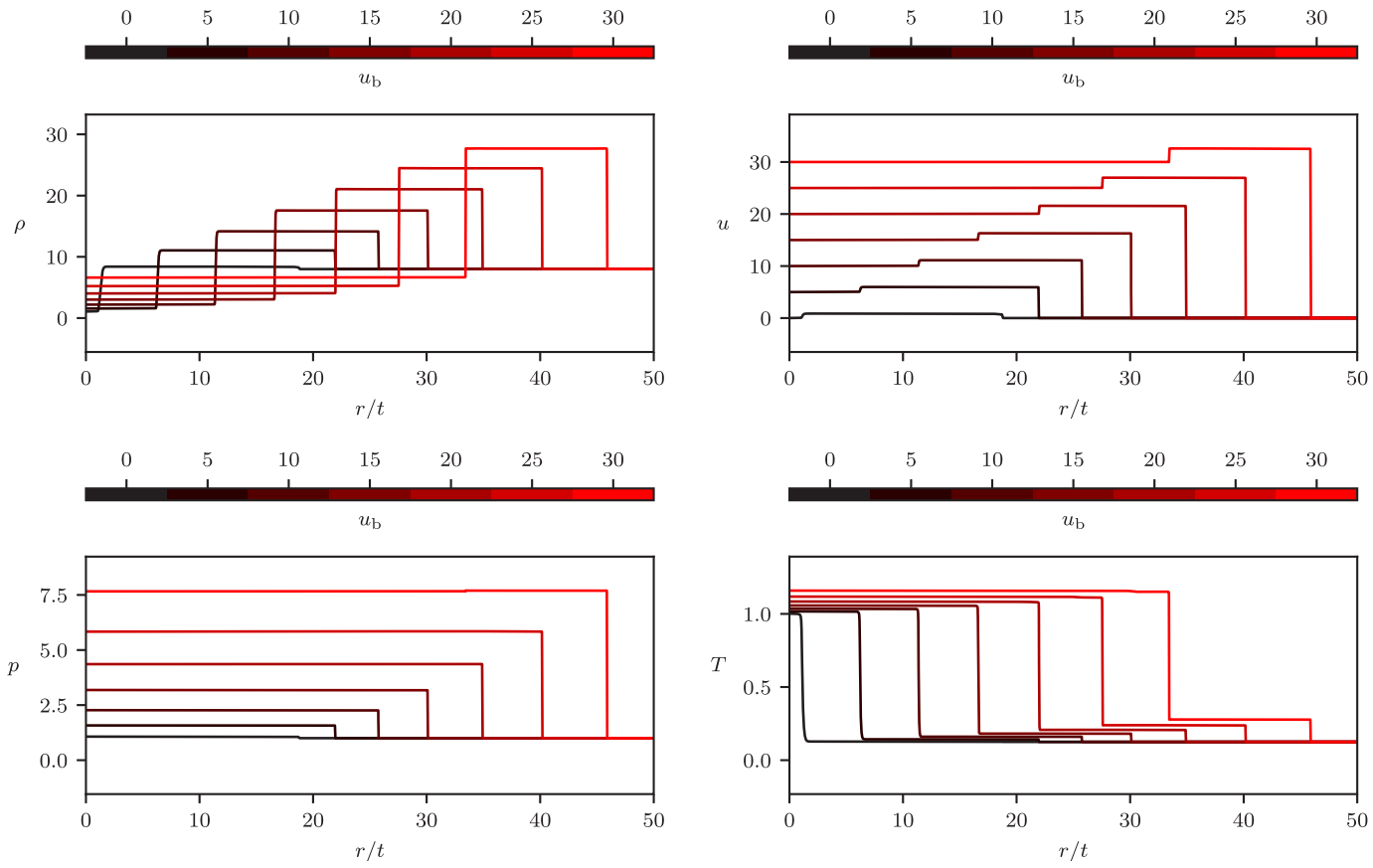

Fig. 4. Density ρ, flow velocity u, pressure p, and temperature T self-similar profiles obtained with the dynamical model after a time lapse of $t = 10$ from initialization for different values of burned gas backflow $u_b = 0, 5, 10, 15, 20, 25$ and 30 (black to red). (For interpretation of the references to color in this figure legend, the reader is referred to the web version of this article.)

propagation velocity in terms of the thermochemical properties of the mixture is then obtained as

$$\frac{u_f^*}{a_o} = \frac{1}{\gamma - 1}\left[\left(1 + \frac{2}{\tilde{b}}\right)^{1/2} - 1\right] \tag{18}$$

which is represented in Fig. 3 by the dotted horizontal line. An expansion of this expression in powers of $\tilde{b}$ to the first order for a large activation energy $\tilde{b} \gg 1$ results in the expression $u_f^*/a_o = \left[(\gamma - 1)\tilde{b}\right]^{-1}$ from the analysis in [40].

4. Dynamical model and internal flame structure

In order to investigate the relevance of the curves obtained with the double discontinuity model as well as the behavior of a finger flame beyond the turning point, numerical simulations have been performed on a dynamical model which can reproduce the internal flame structure. The model is governed by the conservation laws Eqs. (2)–(5) with a finite reaction rate Eq. (6) and the backflow of burned gases behind the flame given by Eq. (1). Thermochemical parameters of the reactive mixture employed in the numerical simulations are specified as Pr = 0.7, Le = 1, $q = 0.875$, $M_{bo} = 2 \times 10^{-2}$, $\beta_o = 10$ and $\vartheta = 2$. A semi-infinite domain is considered subject to the moving wall boundary conditions [46] on the tube closed end

$$\frac{\partial T}{\partial x}(0,t) = \frac{\partial Y}{\partial x}(0,t) = 0, \qquad u(0,t) = u_b, \tag{19}$$

and the far-field conditions at the open end of the tube

$$T(\infty,t) + q = Y(\infty,t) = p(\infty,t) = \rho(\infty,t)T(\infty,t) = u(\infty,t) + 1 = 1. \tag{20}$$

4.1. Steady flame propagation

The nonlinear relationship obtained for the self-similar solution for a quasi-steady regime has been first investigated through a parametric study for a fixed backflow of burned gases in the range $u_b = 0 - 30$. The numerical computation is initialized with the external solution of the large activation energy asymptotic analysis [45] consisting of a preheat region and a reactive layer. In the preheat region, the reactive mixture is heated up by conduction and mixed with the reaction products due to molecular diffusion. While the reactive layer is reduced in this limit to a discontinuity where the release of reaction heat reaction produces a slope jump in the state variables. The initial conditions within the preheat zone of the flame are

$$T(x,0) = T_b - q\left[1 - \exp\left(-\frac{x}{l_f}\right)\right] \tag{21}$$

$$Y(x,0) = \exp\left(-\frac{x\mathrm{Le}}{l_f}\right) \tag{22}$$

$$\rho(x,0) = \frac{\rho_b T_b}{T(x,0)} \tag{23}$$

$$u(x,0) = u_b + \left[1 - \frac{\rho_b}{\rho(x,0)}\right] U_b \tag{24}$$

where the flame thickness scales inversely with the mass flow rate through the flame $l_f = 1/\left(\rho_b U_b\right)$.

Fig. 4 shows density, flow velocity, pressure and temperature profiles in the self-similar independent variable at $t = 10$ from the start of the simulation. The profiles for seven different values of the backflow of burned gases corresponding to different self-similar solutions are represented. The flame and shock wave appear, in these profiles, as discontinuities due to disparity between their length scale and the

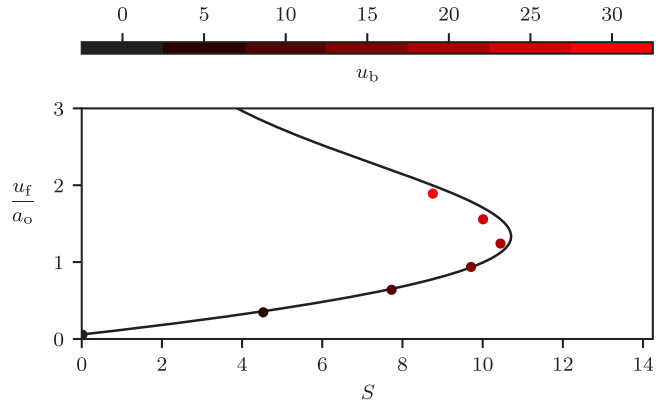

Fig. 5. Flame propagating velocity to sound speed ratio u_f/a_o as a function of the flame elongation parameter S. Colored full points: numerical results of the dynamical model for different constant values of burned gases backflow $u_b = 0, 5, 10, 15, 20, 25$ and 30 (black to red). Black line: curve obtained with the double discontinuity model. (For interpretation of the references to color in this figure legend, the reader is referred to the web version of this article.)

size of the region of uniform flow separating them. While the shock wave corresponds to the discontinuity on the right side of the profile characterized by the intense pressure increase, the flame is shown by the discontinuity at the left side of the profile with an indistinguishable pressure jump and a marked temperature jump. In the absence of burned gas backflow (i.e. $u_b = 0$), the leading shock wave is weak and hardly alters the fresh gas conditions. However, as the backflow of burned gases increases, the impact of the shock wave on the unburned reactive mixture gets more significant. It must also be noted that the self-similar coordinate r/t at which the discontinuities are located represents the dimensionless velocity of propagation of the discontinuity.

Fig. 5 depicts the absolute velocity of the steady flame $u_f = \mathrm{d}r_f/\mathrm{d}t$ against the elongation parameter $S = u_b/U_b$ for the different values of the backflow of burned gases u_b. The nonlinear relationship obtained using the double-discontinuity model for the same set of thermochemical parameters has been included in the figure for comparison. Good agreement is observed between the results from the parametric study (full points) and the curve obtained through the double-discontinuity model. Only small discrepancies can be noticed for fast flames that can be attributed to the departure from the assumption of isobaric flame with increasing burning velocities. Furthermore, it is verified the absence of steady solutions of the model that exceed a critical flame elongation.

4.2. Quasi-steady elongating flame

The dynamics of the flame skirt involves the behavior of a flame propagating within a boundary layer characterized by a complex interplay of compressible fluid dynamics and flame quenching due to heat losses, strained flow, and wall-interaction chemical kinetics. In order to improve the understanding of the velocity runaway phenomenon at the tip of the flame, this aspect has been excluded from the current investigation. As a first approach to modeling the evolution of the flame surface, a linear temporal evolution has been considered to explore the dynamics of the one-dimensional problem around the turning point of the quasi-steady solutions. Experimental results, such as those reported by Krivosheyev et al. [47] and Liberman et al. [24], support the adequacy of the linear approximation, given the observed linear increase in velocity immediately following the exponential regime described by Clanet and Searby [42] and Akkerman et al. [44]. Indeed, a possible explanation for the transition from the initial exponential acceleration to a more linear-like acceleration is offered in [48], where it is attributed to the eventual onset of gas compression effects.

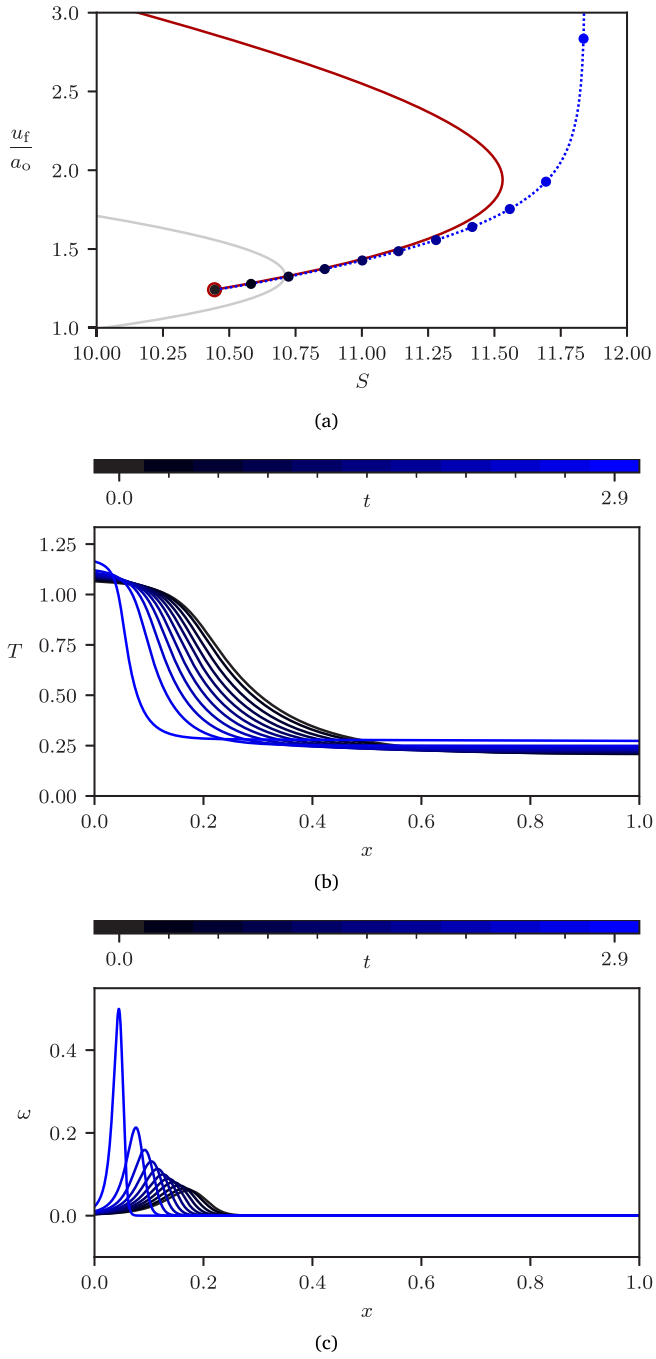

Fig. 6. Flame propagation with a flame elongation S that follows the law given by Eq. (25) with $S_0 = 10.41$. (a) Flame propagating velocity to sound speed ratio u_f/a_o as a function of the flame elongation parameter S. Solid line: double discontinuity solution with an unsteady compression wave corresponding to a burned gas flow of $u_b = 20$. Dotted blue line: flame propagating velocity to sound speed ratio obtained by numerical integration of Eqs. (2)–(5) with a linearly increasing flame elongation parameter over time. The full points from black to blue correspond to the time steps shown in Fig. 6(b). (b,c) Temperature and reaction rate profiles in the flame-attached coordinate system for a slowly elongating flame initialized with the internal flame structure of the self-similar solution for an initial backflow of burned gases of $u_b = 20$. The profiles evolve from $t = 0$ (black) to $t = 2.9$ (blue) in time steps of $\Delta t = 0.29$ and they are represented in the flame-attached coordinate system $x = r - r_f(t)$ with $r_f(t)$ defined as the position of the reactant mass fraction isovalue $Y = 0.02$. (For interpretation of the references to color in this figure legend, the reader is referred to the web version of this article.)

The flame elongation is assumed to be a linearly increasing function of time on a timescale t'_S much larger than the transit time of the flame

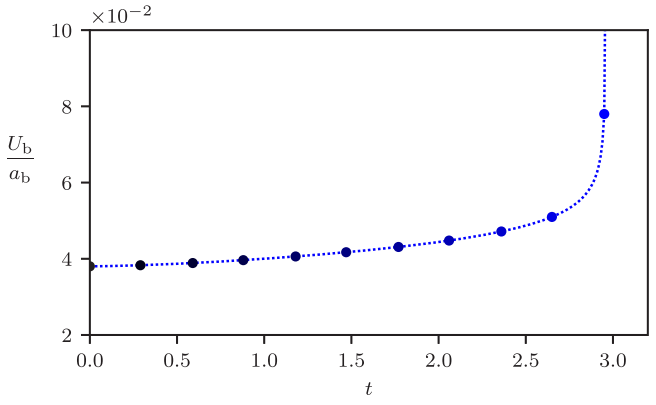

Fig. 7. Time evolution of the flame velocity relative to the burned gases flow with respect to the local sound speed. The flame velocity runaway occurs for a reactive wave that remains significantly subsonic $U_b/a_b \approx 10^{-1} < 1$. The full points indicate the instant corresponding to the profiles steps shown in Fig. 6(b). (For interpretation of the references to color in this figure legend, the reader is referred to the web version of this article.)

$$S(t) = S_0(1 + \epsilon t), \tag{25}$$

where $\epsilon = t'_{fo}/t'_S = 5 \times 10^{-2}$ is the small, but finite, parameter characterizing the ratio of transit time to characteristic evolution time and S_0 is the initial flame elongation parameter at $t = 0$.

The dynamical model with a time-dependent backflow of burned gases prescribed by Eq. (1) and the flame elongation evolution given by Eq. (25), have been numerically simulated. The unsteady evolution of the internal flame structure with an evolving thickness hinders the determination of a well-defined flame speed with respect to the burned gases. To address this issue, the velocity of the flame controlling the backflow of burned gases is computed using Eq. (14) for the equivalent burned gas temperature of the fresh mixture located at the isovalue $1 - Y = 10^{-4}$.

The numerical integration is initialized using the flame structure obtained from the numerical integration of the steady flame propagation with a fixed value of the backflow of burned gases. An example of the numerical results obtained for an initial backflow of burned gases of $u_b = 20$ which corresponds to an initial elongation of $S_0 = 10.41$ is presented in Figs. 6 and 7. The flame velocity as a function of the elongation parameter is compared in Fig. 6(a) with the relationship obtained for the double discontinuity model and the evolution of the temperature profile is plotted in Fig. 6(b) in the flame-attached coordinate system, with the origin located at the reactant mass fraction isovalue of $Y = 0.02$.

The numerical results indicate that the flame accelerates progressively due to both the piston-like effect of the backflow and the temperature sensitivity of the flame burning speed. Initially, the slow increment on the elongation parameter S acts increasing the backflow of burned gases, resulting in a faster flame propagation due to the faster flow velocity, i.e., the flame is advected by a faster gas flow. Simultaneously, the increment in the backflow generates a compression wave that heats up the fresh mixture, thereby accelerating the flame burning velocity relative to the flow.further the flame. As illustrated in Fig. 6(a), once the turning point of the solutions of the double-discontinuity model is surpassed, the flame undergoes a limitless acceleration which corresponds with the finite time singularity analyzed by Clavin [40].

Figs. 6(b) and 6(c) depict the internal structure of the flame during its unsteady evolution, where temporally equispaced temperature profiles are plotted alongside the reaction rate distribution at the same instant in the flame-attached coordinate system. Despite being imperceptible in the temperature profiles, the temperature increase due to compressive heating progressively accelerates the flame up to a velocity runaway, owing to the strong temperature sensitivity. The temperature increase has a more pronounced effect on the thickness of the flame, which abruptly shrinks at the velocity runaway, posing a significant challenge for numerical integration methods based on a discretization of the spatial domain.

It is important to note that within the present model, the flame velocity relative to the burned gases is markedly subsonic $U_b^*/a_b^* \ll 1$ at the velocity runaway. Fig. 7 illustrates the evolution of the flame velocity relative to the burned gases for the specific example of numerical integration presented in this section. Even at the runaway, the flame velocity relative to the burned gases remains ten times slower than the local sound speed. Hence, the velocity runaway takes place well before the marginal solution for reactive waves characterized by the Chapman–Jouguet (CJ) condition is reached.

4.3. Onset of the detonation

The temperature and reactant mass concentration profiles within internal structure of the flame during the acceleration runaway leading to the onset of the detonation are depicted in Figs. 8(b) and 8(c), where the evolution of the flame is illustrated. As the simulation progressed from $t = 2.985$ to $t = 2.990$, the flame continues to accelerate and its internal structure becomes increasingly thin. However, between $t = 2.990$ and $t = 2.991$, a sudden transition in the propagating regime is observed. The flame preheat region, where the fresh mixture is gradually heated by conduction, disappears and the physical variables evolve rapidly within a few grid points from the upstream state to a state of higher temperature and pressure in chemical equilibrium. This sharp transition can be interpreted as a discontinuity in which the mixture undergoes simultaneously compression and burning, as in a detonation in the limit of infinitely fast chemical reaction.

It is worth mentioning that during the numerical integration, only the results obtained every $\Delta t = 0.001$ are stored and included in these figures. However, the CFL stability condition imposes a much finer time resolution, reaching values as small as $\Delta t = 1 \times 10^{-6}$ during the simulation. Therefore, the profiles shown for $t = 2.991$ are not direct results of integrating the conservation equations at $t = 2.990$, but rather a large number of computational steps have taken place in between.

The transition from diffusion-controlled propagation of the flame to detonation might be explained as follows. During the acceleration runaway, as the flame experiences strong acceleration and its internal structure shrinks, the velocity gradient within the internal flame structure steepens, causing viscous dissipation mechanisms that are negligible at ordinary flame velocities to become significant. These viscous dissipation mechanisms eventually result in the formation of a strong shock wave within the internal structure of the flame, which rapidly increases the temperature and further accelerates the reaction rate. The reactants get consumed in a vanishingly thin reactive layer, causing the position of the isovalue $Y = 10^{-4}$, where the temperature is measured to calculate the backflow of burned gases, to be swept out by the reactive supersonic wave. Due to the supersonic nature of the wave, the heat released within the reactive layer cannot propagate ahead, causing the temperature at the isovalue to be determined exclusively by the upstream conditions, which become isolated from what happens behind the supersonic wave. As a result, the temperature at the isovalue does not increase further due to the effect of the compression wave, but is instead propagated into regions of fresher reactive mixture, leading to a slowdown in the backflow of burned gases. However, once the reactive supersonic wave is established it continues to propagate without the piston-like effect of the burned gas backflow.

The evolution of the velocity of the front with respect to the sound speed is plotted in Fig. 8(a), with the time instants corresponding to the profiles in Figs. 8(b) and 8(c) indicated by colored full points. The onset of the detonation coincides with the maximum velocity of the front. It is worth to remember that the data included in the

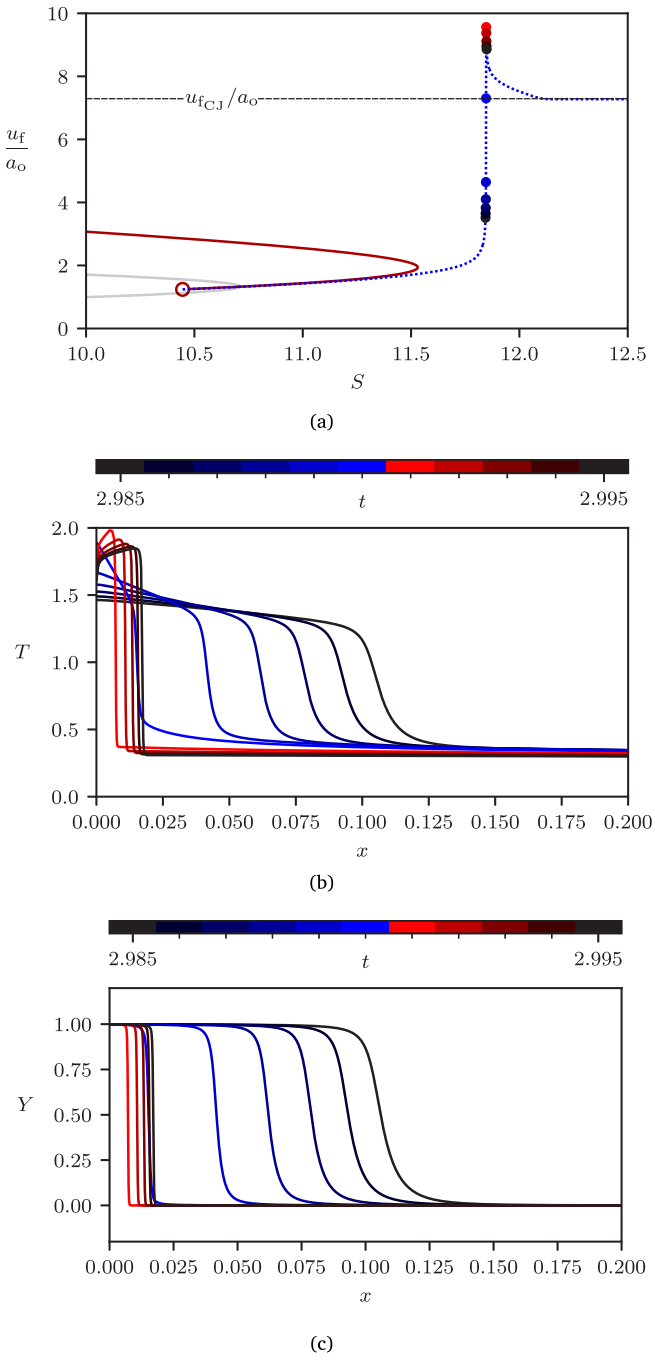

Fig. 8. Onset of the detonation. (a) Flame propagating velocity to initial sound speed ratio as a function of the flame elongation parameter S. The colored circles in both figures correspond to the time steps for the profiles in Figs. 8(b) and 8(c). The horizontal dashed line corresponds to the propagation velocity of a CJ detonation with respect to the initial sound speed considering the flow induced by the expansion ahead of the wave as given by Eq. (26). (b,c) Temperature and reactant mass concentration profiles in the flame-attached coordinate system during the onset of the detonation. The profiles shown evolve from $t = 2.985$ to $t = 2.995$ in time steps of $\Delta t = 0.001$ with the onset of the detonation taking place between $t = 2.990$ (blue) and $t = 2.991$ (red), and they are represented in the flame-attached coordinate system $x = r - r_f(t)$ with $r_f(t)$ defined as the position of the product mass fraction isovalue $Y = 0.98$. (For interpretation of the references to color in this figure legend, the reader is referred to the web version of this article.)

figures does not include every time step of the simulation but just the stored solutions. Consequently, the peak velocity of the flame at the moment of shock formation may actually be significantly higher than the maximum shown in the figure.

The maximum flame velocity included in these results corresponds to the first sample stored following the regime transition. Upon the transition, the flame velocity experiences a slowdown for two reasons. On the one hand, once the front becomes supersonic it advances faster than the compression waves emitted by the flame and then it overtakes the compression waves causing the velocity of the flow ahead of it to decrease, reducing the absolute flame velocity due to the advection of the flow. On the other hand, for the same reason, the temperature of the flow ahead of the supersonic wave decreases, resulting in a reduction of the stable propagation velocity of the supersonic reactive wave.

Once the supersonic wave reaches the head of the compression wave, temperature and flow velocity ahead of it become uniform, leading to a constant propagation velocity. This constant absolute speed is actually equal to the CJ detonation regime, augmented by the velocity of the flow ahead of the wave induced by the leading shock. In the notation followed in this article, this velocity is given by the expression

$$\frac{u_{f_{CJ}}}{a_o} = \frac{D_{CJ}}{a_o} + \frac{u_N}{a_o} = \sqrt{\frac{\gamma+1}{2}\frac{q}{1-q} + \frac{T_N}{1-q}} + \sqrt{\frac{\gamma+1}{2}\frac{q}{1-q}} + \frac{u_N}{a_o} \tag{26}$$

whose numerical application is represented by the dotted horizontal line in Fig. 8(a) showing great agreement.

5. Conclusions

In this study, we have analyzed numerically the impact of a backflow of burned gases on a laminar flame by means of a one-dimensional model. In the context of a flame propagating along a thin tube from a closed end this backflow is caused by the expansion of combustion products close to the tube walls. The backflow is the key element that leads to a flame acceleration runaway, which is a plausible mechanism for DDT. The key feature of this mechanism is a double feedback loop that involves the thermal sensitivity of the flame speed, compressive heating in the flow induced ahead of the flame, and the emergence of the backflow of burned gases in semi-confined geometries that increases the velocity of the gas flow upon which the flame advances. Therefore, the induced flow ahead of the flame increases likewise.

Initially, this study focuses on investigating the solutions for a shock-flame ensemble, when the flame is assumed to be in steady-state. As in flames propagating from a closed end tube, this configuration is known to generate compression waves ahead of the flame that eventually collapse to form a shock wave moving away from the flame. Considering the flame as a steady reactive isobaric discontinuous wave, and the shock wave as a supersonic inert discontinuous wave, the external flow in between has a self-similar solution. The curve of steady solutions as a function of the flame elongation exhibits a turning point that indicates the existence of critical conditions. Above the critical elongation value at which the turning point is found, there is no steady solution, which suggests a possible propagation regime transition.

The turning point also indicates a fast flame acceleration. In the vicinity of this turning point, the flow separating the flame and the shock wave cannot be assumed to be uniform. The difficulty of describing the unsteady flow between the shock wave and the flame has been avoided by limiting the scope of this work to a hypothetical situation in which the compression wave emitted from the flame does not reach the precursor shock wave. The flow separating the flame and the shock wave can then be considered homentropic. By using the isentropic compression relationship between the induced flow and its temperature, a qualitatively similar turning point for the shock-flame ensemble model is obtained. In this case, the critical velocity of the flame is universal (it depends exclusively on the reactive mixture properties), while its critical elongation decreases with the intensity of the leading shock wave.

The relevance of the solutions obtained considering the flame as a reactive discontinuity is confronted with numerical simulations considering a finite reaction rate. For a constant flame elongation, which results in a constant backflow of burned gases, the solutions obtained using a finite reaction rate closely match the solution for a discontinuous flame, proving the emergence of a turning point and the significance of the self-similar solution. When the flame elongation is slowly increased at the characteristic time-scale of the flame, different behaviors are gradually observed. Initially, the relationship between the finite-rate flame speed and flame elongation follows closely the solution for a discontinuous flame. When approaching the turning point, the flame can no longer be considered in steady state due to the rapid acceleration and both solutions move away slightly. After passing the turning point, a rapid flame acceleration is produced. This flame acceleration runaway is coupled with a significant shrinkage of the flame thickness. Finally, an abrupt change is observed in the structure of the reactive front accompanied by the end of the acceleration phase and followed by a relaxation towards the corresponding CJ detonation regime. Both the acceleration of the flame and its shrinkage contribute positively to a local enhancement of the viscous dissipation mechanism causing the formation of a shock wave within the flame structure that leads to the onset of a detonation.

The numerical results illustrate the flame acceleration runaway phenomenon when the flame elongation surpasses the critical value at the turning point of the steady solutions. However, strictly speaking, the relevance of numerical simulations based on the integration of the Navier–Stokes conservation equations during the onset of the detonation is to be questioned. The formation of a shock wave involves spatiotemporal scales corresponding to the mean free path and the elastic collision frequency, for which the continuum and local equilibrium approximations are no longer accurate. Thus, the numerical results presented here cannot prove an accurate description of the instant of detonation onset.

Within the framework of the Navier–Stokes equations, it can only be concluded that the thermal feedback of the compression waves on the flame speed leads to a finite-time singularity, which is likely to result in the formation of a shock wave at the flame tip. If true, this conjecture would mean that a flame propagating faster than the critical velocity $u_f > u_f^*$ is a sufficient condition for the onset of a detonation in the DDT process and that the predetonation time should be close to the time needed by the flame elongation to exceed the corresponding critical value. It should also be noted that the laminar flame speed, the speed at which the reactive front penetrates the moving reactive mixture, remains well below the sound speed before passing the point of no return, contrary to what has been reported in previous works using different one-dimensional flame models.

CRediT authorship contribution statement

Raúl Hernández-Sánchez: Writing – review & editing, Writing – original draft, Visualization, Validation, Software, Methodology, Investigation, Formal analysis. **Bruno Denet:** Writing – review & editing, Supervision, Resources, Project administration, Funding acquisition.

Declaration of competing interest

The authors declare that they have no known competing financial interests or personal relationships that could have appeared to influence the work reported in this paper.

Acknowledgments

The authors are grateful to Paul Clavin, Hassan Tofaili, Luc Vervisch and Guido Lodato for enlightening discussions. Financial support of ANR (*Agence National de la Recherche*) under the project ANR-18-CE05-0030 'ReDDT' (Revisiting Deflagration to Detonation Transition in the context of carbon-free energy production) is acknowledged.

Table A.1
Resolution test $u_b = 20$.

	N	Δr	u_f/a_o
1	35	0.028571	1.242435
2	50	0.02	1.241702
3	70	0.014285	1.241523
4	100	0.01	1.240842
5	140	0.007142	1.240919
6	200	0.005	1.240771

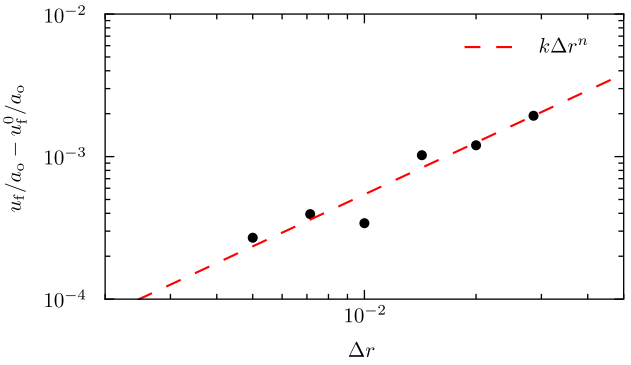

Fig. A.9. Resolution test. Black circles represent the difference between the flame propagation velocity u_f obtained for decreasing spatial steps $\Delta r \in [0.028571, 0.005]$ and the limiting value u_f^0/a_o obtained for $\Delta r \to 0$. The red dashed line is the fitting curve $u_f/a_o - u_f^0/a_o = k\Delta r^n$ obtained for $u_f^0/a_o = 1.240516$, $k = 0.147339$, and $n = 1.221137$.

Appendix. Numerical details and resolution test

The dynamical model governed by Eqs. (2)–(5) is simulated numerically following a Strang splitting algorithm $\boldsymbol{u}^{n+1} = \mathscr{D}^{(\Delta t/2)}\mathscr{C}^{(\Delta t)}\mathscr{D}^{(\Delta t/2)}(\boldsymbol{u}^n)$ where $\boldsymbol{u}^n$ is the vector of conserved quantities $\boldsymbol{u} = (\rho, \rho u, \rho E, \rho Y)$ at the time step n, $\mathscr{D}$ is the diffusion–reaction operator and $\mathscr{C}$ is the convective operator. Application of the diffusion–reaction operator is approximated by an implicit finite difference scheme in which diffusive terms are substituted by central differences, time derivatives are replaced by backward differences and the reactive and dissipative terms are approximated explicitly. The convective operator is applied through the high-resolution central solver for nonlinear conservation laws [49] to integrate the convective terms of the equations.

The computational domain $0 < r < \infty$ is uniformly divided in N computational points per characteristic length scale of the flame thickness t_{fo} resulting in a dimensionless spatial step of $\Delta r = 1/N$. The thickness of the reactive layer being a term $\mathcal{O}(l_f/\beta_o)$ according to the asymptotic analysis of Zel'dovich et al. [10], a lower limit $N > N_{min} = 1/\beta_o$ must be imposed in order to consider the smallest scale of the problem.

The precision of the numerical integration is governed by the spatial discretization Δr. A resolution test is then required to ensure the convergence of the numerical scheme. In this work, the convergence test has been applied to the flame propagation velocity u_f/a_o in the form

$$u_f/a_o \simeq u_f^0/a_o + k\Delta r^n \tag{A.1}$$

where u_f^0/a_o represents the predicted flame velocity in the limit of an infinitesimally small spatial step $\Delta r \to 0$, k is a constant of proportionality, and n is the degree of convergence.

An example of the resolution test for a backflow of burned gases $u_b = 20$ considering an increasing number of computational points per unit length $N_{j+1} \approx \sqrt{2}N_j$ rounded to the closest integer is shown below. Table A.1 summarizes the result of the convergence test which are represented in Fig. A.9. The three fitting parameters u_f^0/a_o, k and n, from the relation are determined using the non-linear least squares method. The predicted limiting value of the propagation velocity is

$u_f^0/a_o = 1.240501$ which differs by 0.02 % from the most resolved simulation. The simulation that considers 200 computational points per unit length provides thus good enough accuracy for the purposes of the present qualitative study.

References

[1] G. Ciccarelli, S. Dorofeev, Flame acceleration and transition to detonation in ducts, Prog. Energy Combust. Sci. 34 (4) (2008) 499–550, http://dx.doi.org/10.1016/j.pecs.2007.11.002.

[2] E. Mallard, H. Le Chatelier, Sur Les Vitesses de Propagation de l'inflammation Dans Les Mélanges Gazeux Explosifs, C. R. Hebd. Séances l'Acad. Sci. 93 (1881) 145–148.

[3] M. Berthelot, P. Vieille, On the velocity of propagation of explosive processes in gases, C. R. Hebd. Sceances Acad. Sci. 93 (2) (1881) 18–21.

[4] P.A. Urtiew, A.K. Oppenheim, S.O. Saunders, Experimental observations of the transition to detonation in an explosive gas, Proc. R. Soc. Lond. Ser. A Math. Phys. Sci. 295 (1440) (1966) 13–28, http://dx.doi.org/10.1098/rspa.1966.0223.

[5] E.S. Oran, V.N. Gamezo, Origins of the deflagration-to-detonation transition in gas-phase combustion, Combust. Flame 148 (1–2) (2007) 4–47, http://dx.doi.org/10.1016/j.combustflame.2006.07.010.

[6] E.S. Oran, Understanding explosions – From catastrophic accidents to creation of the universe, Proc. Combust. Inst. 35 (1) (2015) 1–35, http://dx.doi.org/10.1016/j.proci.2014.08.019.

[7] P. Clavin, G. Searby, Combustion Waves and Fronts in Flows: Flames, Shocks, Detonations, Ablation Fronts and Explosion of Stars, Cambridge University Press, 2016.

[8] J.H.S. Lee, The Detonation Phenomenon, Cambridge University Press, 2008.

[9] K.I. Shelkin, Influence of the wall roughness on initiation and propagation of detonation in gases, Zh. Eksp. Teor. Fiz. 10 (1940) 823.

[10] Y.B. Zel'dovich, V.B. Librovich, G.M. Makhviladze, G.I. Sivashinskil, On the onset of detonation in a nonuniformly heated gas, J. Appl. Mech. Tech. Phys. 11 (2) (1970) 264–270, http://dx.doi.org/10.1007/BF00908106.

[11] J.H.S. Lee, I.O. Moen, The mechans of transition from deflagration to detonation in vapor cloud explosions, Prog. Energy Combust. Sci. 6 (4) (1980) 359–389, http://dx.doi.org/10.1016/0360-1285(80)90011-8.

[12] B. Deshaies, G. Joulin, Flame-speed sensitivity to temperature changes and the deflagration-to-detonation transition, Combust. Flame 77 (2) (1989) 201–212, http://dx.doi.org/10.1016/0010-2180(89)90037-0.

[13] G. Darrieus, Propagation d'un front de flamme, in: La Technique Moderne and Congrés de Mécanique Appliquée Paris, 1938.

[14] L.D. Landau, Slow combustion theory, Zh. Eksp. Teor. Fiz. 14 (6) (1944) 240–244.

[15] O.C. Kwon, G. Rozenchan, C.K. Law, Cellular instabilities and self-acceleration of outwardly propagating spherical flames, Proc. Combust. Inst. 29 (2) (2002) 1775–1783, http://dx.doi.org/10.1016/S1540-7489(02)80215-2.

[16] D. Bradley, T.M. Cresswell, J.S. Puttock, Flame acceleration due to flame-induced instabilities in large-scale explosions, Combust. Flame 124 (4) (2001) 551–559, http://dx.doi.org/10.1016/S0010-2180(00)00208-X.

[17] V.V. Bychkov, M.A. Liberman, Dynamics and stability of premixed flames, Phys. Rep. 325 (4) (2000) 115–237, http://dx.doi.org/10.1016/S0370-1573(99)00081-2.

[18] T.W. Lee, S.J. Lee, Direct comparison of turbulent burning velocity and flame surface properties in turbulent premixed flames, Combust. Flame 132 (3) (2003) 492–502, http://dx.doi.org/10.1016/S0010-2180(02)00495-9.

[19] I. Brailovsky, G.I. Sivashinsky, Hydraulic resistance as a mechanism for deflagration-to-detonation transition, Combust. Flame 122 (4) (2000) 492–499, http://dx.doi.org/10.1016/S0010-2180(00)00157-7.

[20] L. Kagan, G. Sivashinsky, Autoignition due to hydraulic resistance and deflagration-to-detonation transition, Combust. Flame 154 (1) (2008) 186–190, http://dx.doi.org/10.1016/j.combustflame.2007.11.007.

[21] I. Brailovsky, L. Kagan, G. Sivashinsky, Combustion waves in hydraulically resisted systems, Phil. Trans. R. Soc. A 370 (1960) (2012) 625–646, http://dx.doi.org/10.1098/rsta.2011.0341.

[22] L. Kagan, G. Sivashinsky, Deflagration-to-detonation transition in narrow channels: Hydraulic resistance versus flame folding, Combust. Theory Model. 20 (5) (2016) 798–811, http://dx.doi.org/10.1080/13647830.2016.1178399.

[23] M.H. Wu, M.P. Burke, S. Son, R. Yetter, Flame acceleration and the transition to detonation of stoichiometric ethylene/oxygen in microscale tubes, Proc. Combust. Inst. 31 (2) (2007) 2429–2436, http://dx.doi.org/10.1016/j.proci.2006.08.098.

[24] M. Liberman, M. Ivanov, A. Kiverin, M. Kuznetsov, A. Chukalovsky, T. Rakhimova, Deflagration-to-detonation transition in highly reactive combustible mixtures, Acta Astronaut. 67 (7–8) (2010) 688–701, http://dx.doi.org/10.1016/j.actaastro.2010.05.024.

[25] M. Kuznetsov, M. Liberman, I. Matsukov, Experimental study of the preheat zone formation and deflagration to detonation transition, Combust. Sci. Technol. 182 (11–12) (2010) 1628–1644, http://dx.doi.org/10.1080/00102202.2010.497327.

[26] M.H. Wu, C.-Y. Wang, Reaction propagation modes in millimeter-scale tubes for ethylene/oxygen mixtures, Proc. Combust. Inst. 33 (2) (2011) 2287–2293, http://dx.doi.org/10.1016/j.proci.2010.07.081.

[27] Y. Ballossier, F. Virot, J. Melguizo-Gavilanes, Strange wave formation and detonation onset in narrow channels, J. Loss Prev. Process. Ind. 72 (2021) 104535, http://dx.doi.org/10.1016/j.jlp.2021.104535.

[28] J. Melguizo-Gavilanes, Y. Ballossier, L. Faria, Experimental and theoretical observations on DDT in smooth narrow channels, Proc. Combust. Inst. 38 (3) (2021) 3497–3503, http://dx.doi.org/10.1016/j.proci.2020.07.142.

[29] V. Bykov, A. Koksharov, M. Kuznetsov, V.P. Zhukov, Hydrogen-oxygen flame acceleration in narrow open ended channels, Combust. Flame 238 (2022) 111913, http://dx.doi.org/10.1016/j.combustflame.2021.111913.

[30] Y. Ballossier, F. Virot, J. Melguizo-Gavilanes, Flame acceleration and detonation onset in narrow channels: Simultaneous schlieren visualization, Combust. Flame 254 (2023) 112833, http://dx.doi.org/10.1016/j.combustflame.2023.112833.

[31] D. Liu, Z. Liu, H. Xiao, Flame acceleration and deflagration-to-detonation transition in narrow channels filled with stoichiometric hydrogen-air mixture, Int. J. Hydrog. Energy 47 (20) (2022) 11052–11067, http://dx.doi.org/10.1016/j.ijhydene.2022.01.135.

[32] L. Kagan, G. Sivashinsky, The transition from deflagration to detonation in thin channels, Combust. Flame 134 (4) (2003) 389–397, http://dx.doi.org/10.1016/S0010-2180(03)00138-X.

[33] J.D. Ott, E.S. Oran, J.D. Anderson, A mechanism for flame acceleration in narrow tubes, AIAA J. 41 (7) (2003) 1391–1396, http://dx.doi.org/10.2514/2.2088.

[34] L. Kagan, G. Sivashinsky, Parametric transition from deflagration to detonation: Runaway of fast flames, Proc. Combust. Inst. 36 (2) (2017) 2709–2715, http://dx.doi.org/10.1016/j.proci.2016.09.026.

[35] A. Koksharov, V. Bykov, L. Kagan, G. Sivashinsky, Deflagration-to-detonation transition in an unconfined space, Combust. Flame 195 (2018) 163–169, http://dx.doi.org/10.1016/j.combustflame.2018.03.006.

[36] P.V. Gordon, L. Kagan, G. Sivashinsky, Parametric transition from deflagration to detonation revisited: Planar geometry, Combust. Flame 211 (2020) 465–476, http://dx.doi.org/10.1016/j.combustflame.2019.10.011.

[37] P.V. Gordon, L. Kagan, G. Sivashinsky, Parametric transition from deflagration to detonation revisited: Spherical geometry, Combust. Flame 219 (2020) 405–415, http://dx.doi.org/10.1016/j.combustflame.2020.05.015.

[38] A. Koksharov, L. Kagan, G. Sivashinsky, Deflagration-to-detonation transition in an unconfined space: Expanding hydrogen-oxygen flames, Proc. Combust. Inst. 38 (3) (2021) 3505–3511, http://dx.doi.org/10.1016/j.proci.2020.08.051.

[39] P. Clavin, H. Tofaili, A one-dimensional model for deflagration to detonation transition on the tip of elongated flames in tubes, Combust. Flame 232 (2021) 111522, http://dx.doi.org/10.1016/j.combustflame.2021.111522.

[40] P. Clavin, Finite-time singularity associated with the deflagration-to-detonation transition on the tip of an elongated flame-front in a tube, Combust. Flame 245 (2022) 112347, http://dx.doi.org/10.1016/j.combustflame.2022.112347.

[41] P. Clavin, One-dimensional mechanism of gaseous deflagration-to-detonation transition, J. Fluid Mech. 974 (2023) A46, http://dx.doi.org/10.1017/jfm.2023.751.

[42] C. Clanet, G. Searby, On the "Tulip Flame" phenomenon, Combust. Flame 105 (1) (1996) 225–238, http://dx.doi.org/10.1016/0010-2180(95)00195-6.

[43] B. Ponizy, A. Claverie, B. Veyssière, Tulip flame - the mechanism of flame front inversion, Combust. Flame 161 (12) (2014) 3051–3062, http://dx.doi.org/10.1016/j.combustflame.2014.06.001.

[44] V. Akkerman, V. Bychkov, A. Petchenko, L.-E. Eriksson, Accelerating flames in cylindrical tubes with nonslip at the walls, Combust. Flame 145 (1–2) (2006) 206–219, http://dx.doi.org/10.1016/j.combustflame.2005.10.011.

[45] Y. Zeldovich, D.A. Frank-Kamenetskii, A theory of thermal flame propagation, Acta Phys. Chim. 9 (1938) 341–350.

[46] E.F. Toro, Riemann Solvers and Numerical Methods for Fluid Dynamics: A Practical Introduction, Springer, Dordrecht ; New York, 2009.

[47] P. Krivosheyev, A. Novitski, O. Penyazkov, Flame front dynamics, shape and structure on acceleration and deflagration-to-detonation transition, Acta Astronaut. 204 (2023) 692–704, http://dx.doi.org/10.1016/j.actaastro.2022.10.016.

[48] V. Bychkov, V. Akkerman, D. Valiev, C.K. Law, Role of compressibility in moderating flame acceleration in tubes, Phys. Rev. E. 81 (2) (2010) 026309, http://dx.doi.org/10.1103/PhysRevE.81.026309.

[49] A. Kurganov, E. Tadmor, New high-resolution central schemes for nonlinear conservation laws and convection–diffusion equations, J. Comput. Phys. 160 (1) (2000) 241–282, http://dx.doi.org/10.1006/jcph.2000.6459.